

Modeling and Optimal Control of Hybrid UAVs with Wind Disturbance

Sunsoo Kim¹, Niladri Das² and Raktim Bhattacharya³

Abstract—This paper addresses modeling and control of a six-degree-of-freedom unmanned aerial vehicle capable of vertical take-off and landing in the presence of wind disturbances. We design a hybrid vehicle that combines the benefits of both the fixed-wing and the rotary-wing UAVs. A non-linear model for the hybrid vehicle is rapidly built, combining rigid body dynamics, aerodynamics of wing, and dynamics of the motor and propeller. Further, we design an \mathcal{H}_2 optimal controller to make the UAV robust to wind disturbances. We compare its results against that of PID and LQR-based control. Our proposed controller results in better performance in terms of root mean squared errors and time responses during two scenarios: hover and level-flight.

Index Terms—Hybrid UAVs, VTOL, Aircraft Modeling, \mathcal{H}_2 Optimal Control, Wind Disturbances

I. INTRODUCTION

UNMANNED aerial vehicles (UAVs) have proved useful for both civil and military purposes [1]. Their popularity is increasing in applications such as surveillance, search and rescue operations, inspections, security, aerial photograph and video, mapping, and cargo system management [2]–[4].

Researchers and tech companies are developing different UASs to serve different purposes [5], [6]. We divide UAVs into two categories on the basis of their configurations: the rotary-wing UASs and the fixed-wing UASs. Rotary wing UAVs can take-off, land vertically, and hover at one position [7]. While they need a small space for takeoff and landing, these UAVs can neither move fast nor fly long distances since they are not energy efficient. Compared to them, a fixed-wing of UAV is more power-efficient, hence it can fly for a longer duration of time and for further distance [8]. Despite these advantages, fixed-wing UAVs cannot take-off and land in small spaces because they need a runway to do so. Our proposed hybrid design aims to combine the advantages of the rotary-wing and the fixed-wing design.

There are several hybrid UAV concepts [9] such as a the dual system (combining fixed wing and rotary-wing), the tail-sitter, and the tilt-rotor. We classify these concepts according to their thrust direction. The simplest structure involves a dual system, which is a combination of two thrust directions: vertical and forward. In the tail sitter case, the heading of the vehicle is

same as that of the thrust direction. A tail sitter vehicle takes off vertically and then rotates pitch angle of body for the level flight. Unlike the tail-sitter type, in a tilt rotor/wing type of vehicle, it is the actuators that control the thrust direction. It takes-off, tilts the wing or rotor direction for level flight [10], [11], and lands vertically. For our research, we focus on the dual system type of UAV shown in Fig. 1. This is because the vehicle is mechanically simpler than the other hybrid UAVs and has the capability for VTOL and level flight. This UAV can take-off and land in smaller areas while having a large range of operation.

For the modeling of our hybrid UAV, we start with a conceptual design that satisfies our preliminary requirements. First, we calculate the forces and moments coefficients on the wing using the vortex lattice method (VLM). After this aerodynamic analysis, we move on to the propulsion system. Here, we experimentally gather data on the thrust and torque from motor-propeller pair and generate a lookup table for our final model. Next, we formulate the equations of motions based on rigid body dynamics. We use the detailed 3D model of our vehicle which includes properties like mass and inertia to complete our modeling. To perform simulations on this rigid body, we import the CAD (Computer Aided Design) model and lookup tables generated during propulsion analysis to SimScape [12]. We exploit the built-in functionality of SimScape to import 3D design parameters and experimental data into the dynamic model of our UAV.

For UAV control, we mostly use the PID control method because of its ease of implementation [13]–[15]. However, tuning PID gains to achieve the desired performance is a fairly challenging problem. Experimental methods involving trial and error are used to tune these gains [16], [17]. Thus, when UAVs encounter multiple uncertain stimuli such as wind gust, actuator noise, or just modeling errors, the controller may not work properly. Therefore, we need a more robust controller. Researchers have developed adaptive control algorithms using model identification to handle uncertainties in the inertia and motor failure scenario [18], [19]. They have also applied the robust control methods to handle the uncertainty in the system parameters like mass, inertia [20], and actuator characteristics [21]. However, there is little or no work on controller to reject wind disturbances with \mathcal{H}_2 control. Therefore, in this research, we focus on a robust optimal control of our hybrid UAV, which can reject wind disturbance.

The paper is organized as follows. In section §II, we present modeling of our proposed hybrid UAV. Here, wing and thrust dynamics are presented in detail. This is followed by the control algorithms, i.e. PID, Linear Quadratic Regulator

¹Sunsoo Kim is a Ph.D student in the Department of Electrical and Computer Engineering, Texas A&M University, College Station, TX 77843, USA. Email: kimsunsoo@tamu.edu

²Niladri Das is a Ph.D student in the Department of Aerospace Engineering, Texas A&M University, College Station, TX 77843, USA. Email: niladridas@tamu.edu

³Raktim Bhattacharya is with the Faculty of Aerospace Engineering, Texas A&M University, College Station, TX 77843, USA. Email: raktim@tamu.edu

(LQR), and \mathcal{H}_2 control in section §III. In section §IV, we introduce the simulation setup and show the results, followed by conclusions.

II. MODELING OF THE HYBRID UAV

In this paper, we consider both fixed and rotary wing dynamics for our hybrid UAV. We choose the flying wing shape, which does not have a tail wing as shown in Fig. 1. In this section, we are going to first discuss its design (its payload and flight characteristics), followed by its non-linear dynamics. A linearized dynamics model is also developed at the end of this section.

A. Aircraft Design

Aircraft design is based on the desired capabilities we specify for our vehicle. Our aim is to develop a hybrid UAV which combines the advantages of both fixed wing and rotary wing type UAVs. The desired capabilities of the vehicle are set for a multi-functional application and are listed in Table I. They encompass that which is required broadly for applications such as drone deliveries, air surveillance and aerial photography, etc. We start with an initial configuration. This configuration

TABLE I
VEHICLE DESIRED CAPABILITIES

Type of operation	VTOL	Growth weight	3.2 kg
Flight time	30 min	Range	3 km
Level flight speed	22 m/s	Flight control	Auto Flight

is able to sustain level flight, desired range, and satisfy payload characteristics. The final design of our UAV is selected after aerodynamic analysis of the initial configuration and through successive iterations of analysis.

Aerodynamic stability analysis of the initial hybrid UAV configuration is an important step. We used a numerical method called Vortex lattice method (VLM). This is a university-level technique used in computational fluid dynamics, which aids in the early stages of aircraft design. In this work, AVL (Athena Vortex Lattice) [22], [23] and XFLR5 [24] softwares are used to implement VLM. This numerical method models a wing, the primary lifting surface, as an unbounded thin sheet of discrete vortices and calculates the induced drag and lift coefficients. It is also capable of calculating the air profile around an arbitrary wing with its rudimentary configuration alone.

For our UAV, we create batch codes and check the stability of our preliminary designs, followed by calculating forces and moments coefficients. One can see in Fig. 1 that our UAV does not have a tail wing, for the ease of manufacturing. Hence, achieving longitudinal stability turns out to be the most challenging aspect of our design iterations. To address this problem, we select the re-flexed airfoil, Martin Hepperle (MH) 45 [25] and place the center of gravity (CG) in front of the neutral point (NP). The optimal CG point is finally fixed. The corresponding level flight speed characteristics are shown in Table II.

For other payloads, we place the flight controller over the CG of the vehicle. The flight controller consists of an IMU (Inertial Measurement Unit) with integrated 3 axes accelerometer and gyroscope to measure accelerations and angular velocities. A telemetry radio for communication, RC receivers for manual controls, and a 6-cell LIPO battery for the power supply are placed in the vehicle. To ensure both hover flight and level flight, four propellers with a diameter of 9 inch and one propeller with a diameter 12 inch are chosen, which are rotated by 1100 (kv) brush-less-electric motors. In the following subsection, we are going to first develop the rigid-body dynamics followed by modeling the wing dynamics and the thrust dynamics, which are then all combined to generate the full non-linear model for our proposed UAV.

TABLE II
WING CONFIGURATION

Wing span (b)	120 cm	Wing area (S)	3360 cm ²
Root chord (C_r)	28 cm	Mean Aerodynamics Chord	21.2 cm
Tip chord (C_t)	15 cm	X_{CG}	15 cm
Sweep angle	25 °	Height of winglet	15 cm ²

B. Rigid body dynamics modeling

We used Newton-Euler equations to develop the rigid body dynamics of the UAV. The 6-DoF dynamic model is shown in Fig. 1 with the *inertial frame* (I_x, I_y, I_z) and *body frame* (B_x, B_y, B_z) which follow the North-East-Down (NED) coordinate system. ϕ, θ, ψ are the Euler angles in the inertial frame, and

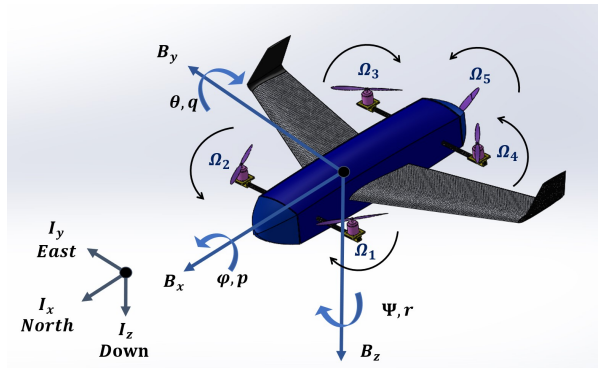


Fig. 1. Hybrid UAV configuration

p, q, r are angular velocities in the body frame about each axis. These 6 variables are the states for the *rotational* motion of the UAV. Similarly, x, y, z are the position in the inertial frame, and u, v, w are velocities in the body frame about each axis. These 6 variables are states for *translational* motion. Hence a total of 12 states of the vehicle dynamics are defined as

$$\mathbf{x} := [x \ y \ z \ u \ v \ w \ \phi \ \theta \ \psi \ p \ q \ r]^T.$$

C. Wing dynamics modeling

The VLM is used to generate the aerodynamic coefficient of the wing body. The vortex lattice methods are based on solutions to Laplace Equation. Although VLM is a classical

method in computational fluid dynamics, it can derive quite accurate results of aerodynamics for 3D Lifting surface, especially, in subsonic flow which we are concerning for modeling [26]. The VLM calculations are mainly processed with the boundary condition and Kutta-Joukowski theorem [27]. The wing is discretized to small panels as Fig. 2. Vortices are placed on each panel and the corresponding strength Γ_i is obtained to satisfy the boundary condition theorem. Finally, forces and moments are computed by the Kutta-Joukowski theorem, which are presented as

$$L_i = \rho V_\infty \times \Gamma_i \Delta b_i \quad (\text{Lift of the panel } i), \quad (1a)$$

$$L = \sum_{i=1}^N L_i \quad (\text{Lift of the Wing}) \quad (1b)$$

$$D_i = \rho V_\infty \times \Gamma_i \Delta b_i \quad (\text{Drag of the panel } i), \quad (1c)$$

$$D = \sum_{i=1}^N D_i \quad (\text{Drag of the Wing}) \quad (1d)$$

where, ρ is the air density, V_∞ is the free stream velocity, Γ_i is the vortex strength in panel i , and b is the length of the vortex segment along the quarter-chord line. The AVL software is

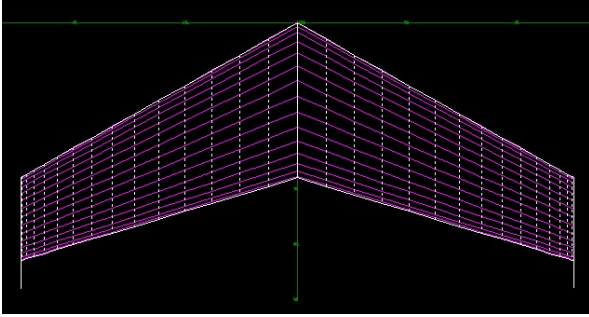


Fig. 2. The vortex lattice method panel

used to obtain the aerodynamic variables of the wing. The result sets, which depend on seven input variables, are made up of a look-up table. The seven input factors are as follows: angle of attack, side slip angle, roll/pitch/yaw rate, elevator, and aileron deflection angle. One of the aerodynamic results from AVL is shown in Fig. 3. The resulting coefficients are then used to calculate the forces and moments for each body axis using

$$F_x = q_\infty S C_{F_x}, \quad F_y = q_\infty S C_{F_y}, \quad F_z = q_\infty S C_{F_z}, \quad (2a)$$

$$M_x = q_\infty S C_{M_x}, \quad M_y = q_\infty S C_{M_y}, \quad M_z = q_\infty S C_{M_z}, \quad (2b)$$

where q_∞ the dynamic pressure is $q_\infty = \frac{1}{2} \rho V_\infty^2$.

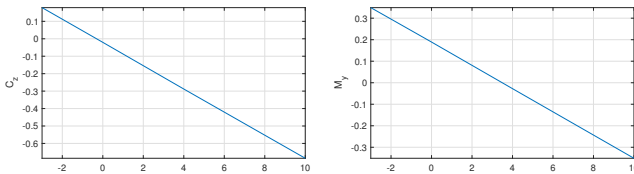


Fig. 3. Aerodynamic coefficient C_Z and M_Y : angle of attack varies from 0 to 10 $^\circ$.

D. Thrust dynamic modeling

Since the hybrid UAV is intended to perform level flights, free stream velocity should be considered when the thrust and torque of propellers are derived. Conventionally, DC motor parameter identification and blade element theory [28] are applied to get dynamic model. However, for more accurate modeling, we use the experimental method to derive brushless DC motor and propellers performance data, wind tunnel test data [29], and generate lookup tables. The result of experiment on brushless DC motor with varying pulse width modulation (PWM) signal input is shown in Fig. 4. The results of thrust and torque from the propeller 12 \times 6 SF (Slow Flight) that depend on wind velocity acting on the wing (free stream velocity) and RPM of motor are shown in Fig 5.

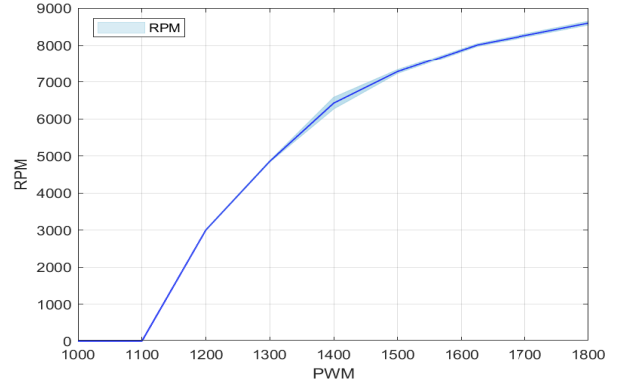


Fig. 4. The motor RPM result from the experiment with motor

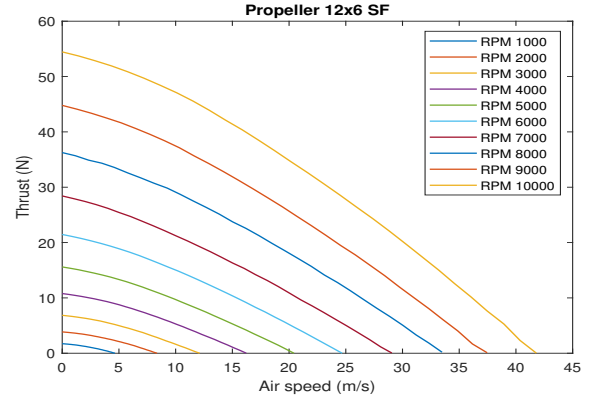


Fig. 5. The propeller thrust from the propeller performance data

E. Final non-linear model

Our hybrid vehicle is developed as a 3D model using CAD. This 3D model which include mass, inertia, and coordinate information is imported to Simscape software in Simulink [12]. The final non-linear 3D model is constructed by combining wing, motor, and propeller dynamics which are previously discussed as shown in Fig. 6. This is the rapid modeling representing the equations of motion of UAVs.

F. Linearized model

We linearize the non-linear model of our hybrid UAV. Our aim is to design the controller for the *attitude control* during

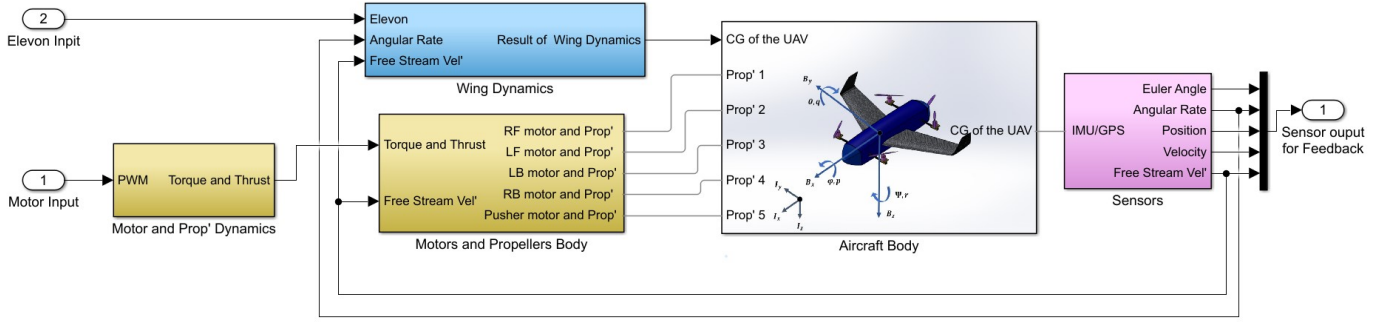


Fig. 6. 6-DOF non-linear simulation of the hybrid UAV

level flight and during hovering. The following linear model is used in designing a \mathcal{H}_2 optimal control to make the system robust to wind gusts. Since we are only interested in attitude control, we consider the corresponding state space $[\theta \ u \ w \ q]^T$ for level flight (Longitudinal motion) and $[\phi \ \theta \ \psi \ p \ q \ r]^T$ for hover flight. We calculate the linearized dynamics separately for level flight and hovering. For level flight, trim states are:

$$p = q = r = 0, \quad V_\infty = 22.49 \text{ m/s}, \quad (3)$$

and for hovering, trim states are

$$p = q = r = 0, \quad u = v = w = 0. \quad (4)$$

The linearized error dynamics about the trim points are modeled as

$$\dot{\mathbf{x}}(t) = \mathbf{A}\mathbf{x}(t) + \mathbf{B}_u\mathbf{u}(t) + \mathbf{B}_w\mathbf{w}(t), \quad (5a)$$

$$\mathbf{y}(t) = \mathbf{C}\mathbf{x}(t), \quad (5b)$$

with states $\mathbf{x} := [\delta\theta \ \delta u \ \delta w \ \delta q]^T$ for level flight and $\mathbf{x} := [\delta\phi \ \delta\theta \ \delta\psi \ \delta p \ \delta q \ \delta r]^T$ for hovering, which are perturbations on states about trim point. The system matrices for level flight are

$$\mathbf{A} = \begin{bmatrix} 0 & 0 & 0 & 0 \\ 0 & 0.0002 & -0.0235 & -0.1360 \\ 0 & 0.0011 & -0.1793 & 20.4845 \\ 0 & 0.0135 & -2.1745 & -3.2657 \end{bmatrix}, \quad \mathbf{B}_u = \begin{bmatrix} 0 \\ 0.0009 \\ -0.0407 \\ -0.6544 \end{bmatrix}, \quad (6)$$

$$\mathbf{B}_w = [0 \ 0 \ 0 \ 1]^T, \quad \mathbf{C} = \mathbf{I}_{4 \times 4},$$

where u is elevon deflection (δ_e). And for hover flight

$$\mathbf{A} = \begin{bmatrix} \mathbf{0}_{3 \times 3} & \mathbf{I}_{3 \times 3} \\ \mathbf{0}_{3 \times 3} & \mathbf{0}_{3 \times 3} \end{bmatrix}, \quad \mathbf{B}_u = \begin{bmatrix} \mathbf{0}_{3 \times 4} \\ -153.5 & 153.5 & 153.5 & -153.5 \\ 36.9 & -37.1 & 36.9 & -37.1 \\ -1.8 & -1.8 & 1.8 & 1.8 \end{bmatrix}, \quad (7)$$

$$\mathbf{B}_w = [0 \ 0 \ 0 \ 1 \ 1 \ 1]^T, \quad \mathbf{C} = \mathbf{I}_{6 \times 6},$$

where u is four motor input ($PWM_i, i = 1 \sim 4$).

III. CONTROL

In this paper, we present a \mathcal{H}_2 optimal controller for our proposed novel hybrid UAV. Our hybrid vehicle harnesses the advantages of both fixed wing and rotor wing UAVs. We consider the following linear system which models the error dynamics about the trim points

$$\dot{\mathbf{x}}(t) = \mathbf{A}\mathbf{x}(t) + \mathbf{B}_w\mathbf{w}(t) + \mathbf{B}_u\mathbf{u}(t), \quad (8a)$$

$$\mathbf{z}(t) = \mathbf{C}_z\mathbf{x}(t) + \mathbf{D}_u\mathbf{u}(t), \quad (8b)$$

$$\mathbf{y}(t) = \mathbf{C}_y\mathbf{x}(t), \quad (8c)$$

where $\mathbf{x} \in \mathbb{R}^{n_x}$, $\mathbf{y} \in \mathbb{R}^{n_y}$, $\mathbf{z} \in \mathbb{R}^{n_z}$ are the state vector, the measured output vector, and the output vector of interest, respectively. Variables $\mathbf{w} \in \mathbb{R}^{n_w}$ and $\mathbf{u} \in \mathbb{R}^{n_u}$ are the disturbances and the control vectors, respectively.

We are interested in designing a full state feedback \mathcal{H}_2 optimal controller for the system in Eq. 8, i.e.,

$$\mathbf{u}(t) = \mathbf{K}\mathbf{x}(t), \quad (9)$$

such that the closed loop system is stable and the effect of the disturbance is attenuated to a desired level. We perform a comparative study of the performance of the \mathcal{H}_2 optimal control with that of the conventional PID control and the LQR, when applied to our system. \mathcal{H}_2 control is expected to achieve better control performance in presence of disturbances since it incorporates the disturbance term \mathbf{B}_w inside the optimization process. Now, we briefly discuss the three controllers.

A. PID controller

PID (Proportional-Integral-derivative) control is a model-free control algorithm. A PID controller calculates an error value as the difference between the desired set point and measured point and then applies a correction based on a proportional, integral, and derivative terms as

$$\mathbf{u}(t) = K_P \mathbf{e}(t) + K_i \int_0^t \mathbf{e}(t') dt' + K_d \frac{d\mathbf{e}(t)}{dt} \quad (10)$$

Most UAV systems currently use the PID controller for attitude control [13]. Feedback measurement or estimated Euler angles and angular velocities [30] are compared with the desired angle and angular velocity, respectively. The PID control generates an input value to eliminate the error. PID control framework for the attitude control is shown in Fig. 7. For PID gain tuning, one can refer to [16], [17], [31] for a more detailed analysis.

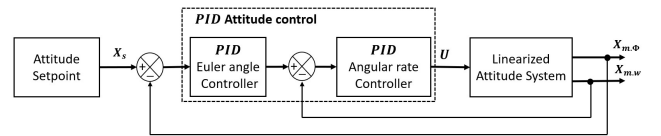


Fig. 7. Attitude control structure of UAVs using of PID control

B. LQR optimal control

The linear quadratic regulator (LQR) is a method used in determining the state feedback controller $u = K_{LQR}x$. This controller is designed to minimize the cost function, J , defined as

$$J = \int_0^{\infty} (x^T Q x + u^T R u) dt \quad (11)$$

where $Q \geq 0$ and $R > 0$ are symmetric weighting matrices. These matrices are the main design parameters for defining the the control objective so that the state error and control energy is minimized. This cost function is solved with MATLAB function `lqr()`. The LQR problem can be converted to the LMI (Linear Matrix Inequality) form as given by the following theorem.

Theorem 1 ([32]): The following two statements are equivalent:

- 1) A solution K_{LQR} to the LQR controller exists.
- 2) \exists a matrix Y , a symmetric matrix W , and a symmetric matrix $Y = P^{-1}$ such that:

$$AY + YA^T + W^T B_u^T + B_u W + Y Q Y + W^T R W < 0 \quad (12)$$

The optimal LQR control gain, K_{LQR} , is determined by solving the following optimization problem.

$$\min_{P, W, Y} \text{trace}(P) \quad \text{subject to (12)}.$$

The gain K_{LQR} is recovered by $K_{LQR} = WY^{-1}$. This optimal gain minimizes the cost function (11). To solve this optimized solution, we used CVX [33] and MATLAB tool box [34].

C. \mathcal{H}_2 Optimal Control

With the linear system (8) and control law (9), the \mathcal{H}_2 control closed-loop has the following form,

$$\dot{x}(t) = (A + B_u K)x(t) + B_z w(t), \quad (13a)$$

$$z(t) = (C_z + D_u K)x(t), \quad (13b)$$

Therefore, the influence of the disturbance w on the output z is determined in frequency domain as $z = G_{zw}(s)w(s)$ where $G_{zw}(s)$ is the transfer function from the disturbance w to the output z given by

$$G_{zw}(s) = C_z(C_z + D_u K)[sI - (A + B_u K)]^{-1} B_w. \quad (14)$$

The problem of \mathcal{H}_2 optimal control design is then, given a system (14) and a positive scalar γ , find a matrix $K = K_{\mathcal{H}_2}$ such that

$$\|G_{zw}(s)\|_2 < \gamma. \quad (15)$$

where $\|G(\cdot)\|_2$ is the corresponding 2-norm of the system. The formulation to obtain $K_{\mathcal{H}_2}$ is given by the following theorem.

Theorem 2 ([32], [35], [36]): The following two statements are equivalent:

- 1) A solution $K_{\mathcal{H}_2}$ to the \mathcal{H}_2 controller exists.

- 2) \exists a matrix W , a symmetric matrix Z , and a symmetric matrix X such that:

$$\begin{aligned} AX + B_u W + (AX + B_u W)^T + B_w B_w^T &< 0 \\ \begin{bmatrix} -Z & C_z X + D_z W \\ * & -X \end{bmatrix} &< 0 \\ \text{trace}(Z) &< \gamma^2 \end{aligned} \quad (16)$$

The minimal attenuation level γ is determined by solving the following optimization problem

$$\min_{W, X, Z} \gamma \quad \text{subject to (16)}.$$

The \mathcal{H}_2 optimal control gain is recovered by $K_{\mathcal{H}_2} = W X^{-1}$.

This optimal gain ensures that the closed-loop system is asymptotically stable and attenuates the disturbance. To solve this optimization problem, we use CVX [33] and Matlab tool box [34]. LQR and \mathcal{H}_2 control framework for the attitude control is shown in Fig. 8.

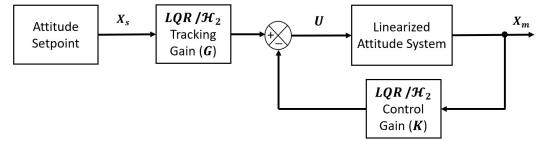


Fig. 8. Attitude control structure of UAVs using LQR and \mathcal{H}_2 controller

IV. RESULTS

A. Simulation set up

The proposed \mathcal{H}_2 optimal control is applied to attitude control of the linearized dynamics of our UAV as modeled by Eq. 5. We compare its performance with the PID controller and LQR. The comparison is done with respect to the control input, system response, and the amount of wind disturbance rejection, in a Simulink based simulation environment, as shown in Fig. 10. In this simulation, the Dryden wind turbulence model was used to generate the wind disturbance. The generated wind disturbance is 10 m/s from north. Angular velocity components of the wind along X and Y axes are shown in Fig. 9. The

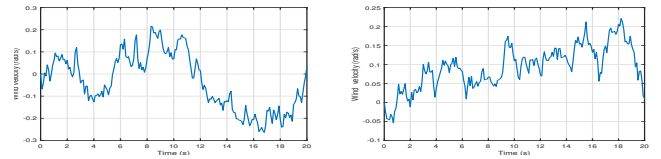


Fig. 9. Angular velocity component of wind disturbance about the X (Left) and Y (Right) axis generated by the Dryden wind turbulence model in the Simulink software.

final simulation environment which includes the UAV system, controller, and disturbance model is shown in Fig. 10.

We simulated two cases: *Case I – Level flight (Longitudinal motion)* which considers parameters in Eq. (6) for level flight trim states in Eq. (3). Input of the system is deflection angle of elevon surface and measurement is angular velocity q . Initial deviation of angular velocity about Y axis in body frame p , is 0.5 rad/sec. *Case II – Hover flight* which consider parameters

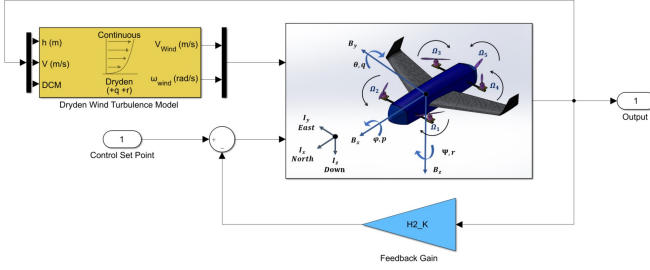


Fig. 10. 6-DOF non-linear simulation of the hybrid UAV with disturbance

in Eq. (7) for hover at trim states in Eq. (4). Input to the system is the PWM signals of four motors and, measurement are all state, Euler angle and angular velocity. Initial deviation of pitch angle θ , is 10° .

LQR (12), PID (10), and \mathcal{H}_2 (16) controllers are designed with these two linearized systems and then tested in the non-linear model in Fig 10.

B. Simulation results

We examine the performance of the \mathcal{H}_2 control by comparing it with that of the PID controller and LQR in terms of root mean squared (RMS) error and time response.

Case I: Level flight – The simulation results for the proposed \mathcal{H}_2 control, the PID, and the LQR are shown in Fig. 11 and TABLE III. The proposed \mathcal{H}_2 control has the least RMS error than the other controllers, as shown in TABLE III. The time response and overshoot of \mathcal{H}_2 control is noted to be shorter than one of the PID controller and the LQR.

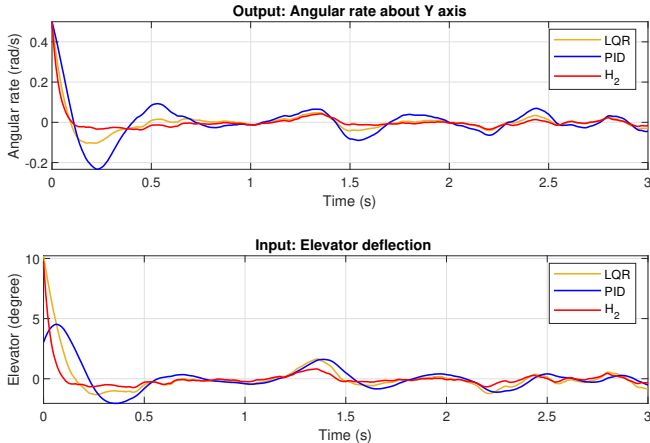


Fig. 11. Error comparison of LQR, PID, and \mathcal{H}_2 control with wind disturbance in level flight

TABLE III
RMS ERROR FOR LEVEL FLIGHT: CASE I.

Algorithm	LQR	PID	\mathcal{H}_2
q (rad/sec)	0.0573	0.0859	0.0457

Case II: Hover flight – The simulation results for the proposed \mathcal{H}_2 control, PID, and the LQR are shown in Fig. 12 and TABLE IV. The proposed \mathcal{H}_2 control has the least

RMS error compared to the other controllers, as shown in TABLE IV, especially in yaw angle (ψ). The time response of proposed \mathcal{H}_2 control is comparable with one from the PID controller and LQR. Here, note that \mathcal{H}_2 is implicitly a better algorithm to deal with disturbance since it include disturbance as a design factor.

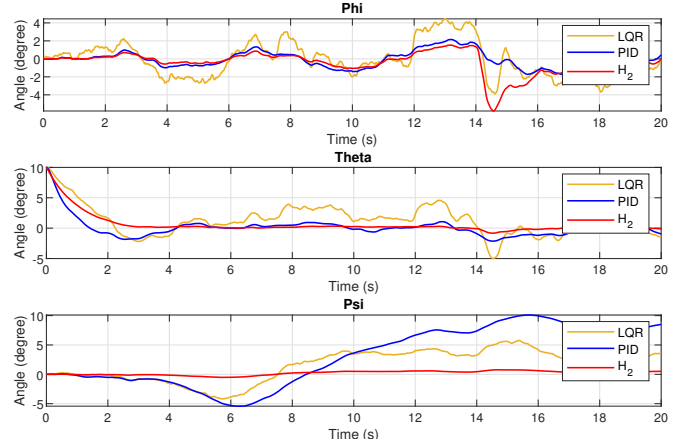


Fig. 12. Error comparison of LQR, PID, and \mathcal{H}_2 control with wind disturbance in Hover flight

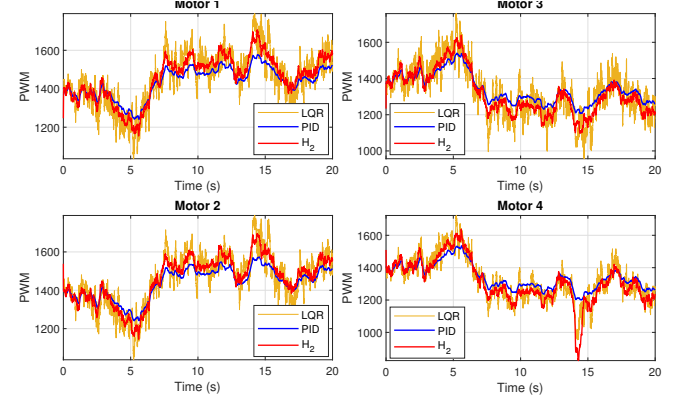


Fig. 13. Input comparison of LQR, PID, and \mathcal{H}_2 control with wind disturbance in hover flight

TABLE IV
RMS ERROR FOR THE HOVER FLIGHT: CASE II.

Algorithm	Roll angle ($^\circ$)	Pitch angle ($^\circ$)	Yaw angle ($^\circ$)
LQR	0.8964	1.9441	3.0217
PID	0.0349	1.3169	5.7745
\mathcal{H}_2	0.1878	1.5935	0.4370

V. CONCLUSION

This paper presents an approach to design a vertical take-off and landing hybrid UAV. We elaborately describe its modeling and controller design that will make it robust to wind disturbances. We discuss methods that rapidly implements the modeling of our proposed hybrid UAV satisfying the requirements with sufficient accuracy. We also propose

a robust controller based on \mathcal{H}_2 optimal theory for our hybrid UAV. This controller achieves better performance while rejecting wind gusts compared to that of the PID and the LQR controller. For the future work, discrete time system of UAV will be developed and tested in physical UAV model.

REFERENCES

- [1] Shiva Ram Reddy Singireddy and Tugrul U Daim. Technology roadmap: Drone delivery–amazon prime air. In *Infrastructure and Technology Management*, pages 387–412. Springer, 2018.
- [2] US Army. Unmanned aircraft systems roadmap 2010–2035. *US Army UAS Center of Excellence, Fort Rucker, Alabama, USA*, 10:205, 2010.
- [3] Luca Canetta, Gianpiero Mattei, and Athos Guanziroli. Exploring commercial uav market evolution from customer requirements elicitation to collaborative supply network management. In *2017 International Conference on Engineering, Technology and Innovation (ICE/ITMC)*, pages 1016–1022. IEEE, 2017.
- [4] Micha Mazur, A Wisniewski, and J McMillan. Pwc global report on the commercial applications of drone technology. *PricewaterhouseCoopers, tech. Rep.*, 2016.
- [5] Hazim Shakhatreh, Ahmad H Sawalmeh, Ala Al-Fuqaha, Zuochoao Dou, Eyad Almaita, Issa Khalil, Noor Shamsiah Othman, Abdallah Khreishah, and Mohsen Guizani. Unmanned aerial vehicles (uavs): A survey on civil applications and key research challenges. *IEEE Access*, 7:48572–48634, 2019.
- [6] Chun Fui Liew, Danielle DeLatte, Naoya Takeishi, and Takehisa Yairi. Recent developments in aerial robotics: A survey and prototypes overview. *arXiv preprint arXiv:1711.10085*, 2017.
- [7] Hossein Bolandi, Mohammad Rezaei, Reza Mohsenipour, Hossein Nemat, and S. M. Smailzadeh. Attitude control of a quadrotor with optimized PID controller. *Intelligent Control and Automation*, 04(03):335–342, 2013.
- [8] Andrei Dorobantu, Austin Murch, Bérénice Mettler, and Gary Balas. System identification for small, low-cost, fixed-wing unmanned aircraft. *Journal of Aircraft*, 50(4):1117–1130, 2013.
- [9] Adnan S Saeed, Ahmad Bani Younes, Chenxiao Cai, and Guowei Cai. A survey of hybrid unmanned aerial vehicles. *Progress in Aerospace Sciences*, 98:91–105, 2018.
- [10] Burak Yuksek, Aslihan Vuruskan, Ugur Ozdemir, MA Yukselen, and Gökhan Inalhan. Transition flight modeling of a fixed-wing vtol uav. *Journal of Intelligent & Robotic Systems*, 84(1-4):83–105, 2016.
- [11] C. Hancer, K. T. Oner, E. Sirimoglu, E. Cetinsoy, and M. Unel. Robust hovering control of a quad tilt-wing UAV. In *IECON 2010 - 36th Annual Conference on IEEE Industrial Electronics Society*. IEEE, nov 2010.
- [12] MATLAB. Simscape, 2020. [Accessed: 25-Marv-2020].
- [13] Yibo Li and Shuxi Song. A survey of control algorithms for quadrotor unmanned helicopter. In *2012 IEEE Fifth International Conference on Advanced Computational Intelligence (ICACI)*, pages 365–369. IEEE, 2012.
- [14] Atheer L Salih, M Moghavvemi, Haider AF Mohamed, and Khalaf Sallom Gaeid. Modelling and pid controller design for a quadrotor unmanned air vehicle. In *2010 IEEE International Conference on Automation, Quality and Testing, Robotics (AQTR)*, volume 1, pages 1–5. IEEE, 2010.
- [15] Nguyen Xuan-Mung and Sung-Kyung Hong. Improved altitude control algorithm for quadcopter unmanned aerial vehicles. *Applied Sciences*, 9(10):2122, 2019.
- [16] Gaopeng Bo, Liuyong Xin, Zhang Hui, and Wanglin Ling. Quadrotor helicopter attitude control using cascade pid. In *2016 Chinese Control and Decision Conference (CCDC)*, pages 5158–5163. IEEE, 2016.
- [17] Pengcheng Wang, Zhihong Man, Zhenwei Cao, Jinchuan Zheng, and Yong Zhao. Dynamics modelling and linear control of quadcopter. In *2016 International Conference on Advanced Mechatronic Systems (ICAMechS)*, pages 498–503. IEEE, 2016.
- [18] Matthias Schreier. Modeling and adaptive control of a quadrotor. In *2012 IEEE international conference on mechatronics and automation*, pages 383–390. IEEE, 2012.
- [19] Zachary T Dydek, Anuradha M Annaswamy, and Eugene Lavretsky. Adaptive control of quadrotor uavs: A design trade study with flight evaluations. *IEEE Transactions on control systems technology*, 21(4):1400–1406, 2012.
- [20] Shafiqul Islam, Peter X Liu, and Abdulmotaleb El Saddik. Robust control of four-rotor unmanned aerial vehicle with disturbance uncertainty. *IEEE Transactions on Industrial Electronics*, 62(3):1563–1571, 2014.
- [21] Hao Liu, Xiafu Wang, and Yisheng Zhong. Quaternion-based robust attitude control for uncertain robotic quadrotors. *IEEE Transactions on Industrial Informatics*, 11(2):406–415, 2015.
- [22] Mark Drela and Harold Youngren. Athena vortex lattice. *Software Package, Ver*, 3, 2004.
- [23] Tomas Melin. A vortex lattice matlab implementation for linear aerodynamic wing applications. *Royal Institute of Technology, Sweden*, 2000.
- [24] André Deperrois. Xflr5 analysis of foils and wings operating at low reynolds numbers. *Guidelines for XFLR5*, 2009.
- [25] Michael S Selig. Uic airfoil data site, 1996.
- [26] Russell M Cummings, William H Mason, Scott A Morton, and David R McDaniel. *Applied computational aerodynamics: A modern engineering approach*, volume 53. Cambridge University Press, 2015.
- [27] Dale Anderson, Ian Graham, and Brian Williams. Aerodynamics. In *Flight and Motion*, pages 14–19. Routledge, 2015.
- [28] John M Seddon and Simon Newman. *Basic helicopter aerodynamics*, volume 40. John Wiley & Sons, 2011.
- [29] APC Propellers. Apc performance data, 2020. [Accessed: 25-Marv-2020].
- [30] Sunsoo Kim, Vaishnav Tadiparthi, and Raktim Bhattacharya. Nonlinear attitude estimation for small uavs with low power microprocessors. *arXiv preprint arXiv:2003.13802*, 2020.
- [31] Sunsoo Kim, Vedang Deshpande, and Raktim Bhattacharya. H2 optimized pid control of quad-copter platform with wind disturbance. *arXiv preprint arXiv:2003.13801*, 2020.
- [32] Guang-Ren Duan and Hai-Hua Yu. *LMIs in control systems: analysis, design and applications*. CRC press, 2013.
- [33] Michael Grant, Stephen Boyd, and Yinyu Ye. Cvx: Matlab software for disciplined convex programming, 2009.
- [34] Da-Wei Gu, Petko Petkov, and Mihail M Konstantinov. *Robust control design with MATLAB®*. Springer Science & Business Media, 2005.
- [35] Pierre Apkarian, Hoang Duong Tuan, and Jacques Bernussou. Continuous-time analysis, eigenstructure assignment, and h/sub 2/synthesis with enhanced linear matrix inequalities (lmi) characterizations. *IEEE Transactions on Automatic Control*, 46(12):1941–1946, 2001.
- [36] Stephen Boyd, Venkataramanan Balakrishnan, Eric Feron, and Laurent ElGhaoui. Control system analysis and synthesis via linear matrix inequalities. In *1993 American Control Conference*, pages 2147–2154. IEEE, 1993.